Astron. Nachr. / AN **334**, No. 4/5, 360 – 363 (2013) / **DOI** 10.1002/asna.201211857

# A simple recipe for estimating masses of elliptical galaxies and clusters of galaxies

**N. Lyskova**[1,2,⋆]

[1] Max-Planck-Institut für Astrophysik, Karl-Schwarzschild-Straße 1, 85741 Garching, Germany
[2] Space Research Institute (IKI), Profsoyuznaya 84/32, Moscow 117997, Russia

Received 2012 Aug 24, accepted 2012 Sep 17
Published online 2013 May 2

**Key words** galaxies: clusters: general – galaxies: kinematics and dynamics – X-rays: galaxies: clusters

We discuss a simple and robust procedure to evaluate the mass/circular velocity of massive elliptical galaxies and clusters of galaxies. It relies only on the surface density and the projected velocity dispersion profiles of tracer particles and therefore can be applied even in case of poor or noisy observational data. Stars, globular clusters or planetary nebulae can be used as tracers for mass determination of elliptical galaxies. For clusters the galaxies themselves can be used as tracer particles. The key element of the proposed procedure is the selection of a "sweet" radius $R_{\rm sweet}$, where the sensitivity to the unknown anisotropy of the tracers' orbits is minimal. At this radius the surface density of tracers declines approximately as $I(R) \propto R^{-2}$, thus placing $R_{\rm sweet}$ not far from the half-light radius of the tracers $R_{\rm eff}$. The procedure was tested on a sample of cosmological simulations of individual galaxies and galaxy clusters and then applied to real observational data. Independently the total mass profile was derived from the hydrostatic equilibrium equation for the gaseous atmosphere. Mismatch in mass profiles obtained from optical and X-ray data is used to estimate the non-thermal contribution to the gas pressure and/or to constrain the distribution of tracers' orbits.



## 1 Introduction

Reliable mass estimates of individual galaxies and clusters of galaxies play an important role in observational cosmology and studies of galaxy formation and evolution. If the task is to estimate gravitational masses for a large sample of objects perhaps with poor and/or noisy observational data, detailed modelling (e.g., Schwarzschild 1979; Gebhardt & Thomas 2009) is not justified. In such a case it is desirable to have a simple and fast technique that relies only on the most basic observables and provides an unbiased estimate of the mass with reasonable scatter.

As an order of magnitude estimate one can use the virial theorem. For a closed stationary spherical system in an isothermal gravitational potential a circular velocity is related to the average (luminosity-weighted) line-of-sight velocity dispersion as $V_{\rm c}^2 = 3\left\langle\sigma_{\rm p}^2\right\rangle$. Among the advantages of this approach is not only it's simplicity but also an absence of any assumptions about the intrinsic 3D velocity dispersion of tracers. In practice, observed systems are not guaranteed to be closed and/or to have the isothermal gravitational potential. A common approach to weaken these assumptions is to use the Jeans equation relating the anisotropy parameter $\beta$ that quantifies the difference between radial and tangential components of the velocity dispersion tensor, a volume density of tracers $j(r)$ and a radial velocity dispersion $\sigma_r(r)$ together under the assumptions of spherical symmetry of the system and it's dynamic equilibrium with no streaming motions (Binney & Tremaine 2008):

$$\frac{\rm d}{{\rm d}r} j\sigma_r^2 + 2\frac{\beta}{r} j\sigma_r^2 = -j\frac{{\rm d}\Phi}{{\rm d}r}, \tag{1}$$

where $\Phi(r)$ is a gravitational potential of the system, $\beta(r) = 1 - \sigma_\theta^2/\sigma_r^2$ for the spherically symmetric case ($\sigma_\theta(r)$ is the tangential velocity dispersion). For a given $\beta(r)$ one can derive $M(<r)$ from the Jeans equation linking $j(r)$ and $\sigma_r(r)$ to the observable surface brightness $I(R)$ and projected velocity dispersion $\sigma_p(R)$ via

$$I(R) = 2\int_R^\infty \frac{jr\,{\rm d}r}{\sqrt{r^2 - R^2}}, \tag{2}$$

$$\sigma_{\rm p}^2(R) I(R) = 2\int_R^\infty \left(1 - \frac{R^2}{r^2}\beta\right) \frac{j\sigma_r^2 r\,{\rm d}r}{\sqrt{r^2 - R^2}}. \tag{3}$$

Unfortunately, there is no direct and reliable way to derive $\beta(r)$ from observational data without detailed modelling. So it makes sense to find a method still allowing mass determination (even if only at some particular radius only) but with minimal sensitivity to the anisotropy. For instance, such approaches have been discussed in Richstone & Tremaine (1984), Churazov et al. (2010), Wolf et al. (2010), and Lyskova et al. (2012).

## 2 Description of the method

Assuming the logarithmic form of the gravitational potential $\Phi(r) = V_{\rm c}^2 \ln(r) + {\rm const}$ we can solve the Jeans equation coupled with Eqs. (2) and (3) for three types of tracers'

⋆ Corresponding author: lyskova@mpa-garching.mpg.de

orbits: isotropic (in this case $\beta \equiv 0$), radial ($\beta \equiv 1$), and circular ($\beta \to -\infty$).

These relations are given by

$$V_{\rm c}^{\rm iso} = \sigma_{\rm iso}(R)\sqrt{1+\alpha+\gamma}\,,$$
$$V_{\rm c}^{\rm circ} = \sigma_{\rm circ}(R)\sqrt{2\frac{1+\alpha+\gamma}{\alpha}}\,, \quad (4)$$
$$V_{\rm c}^{\rm rad} = \sigma_{\rm rad}(R)\sqrt{(\alpha+\gamma)^2+\delta-1}\,,$$

where

$$\alpha = -\frac{{\rm d}\ln I}{{\rm d}\ln R},\ \ \gamma = -\frac{{\rm d}\ln \sigma^2}{{\rm d}\ln R},\ \ \delta = \frac{{\rm d}^2\ln(I\sigma^2)}{{\rm d}(\ln R)^2}. \quad (5)$$

If the dispersion velocity profile is too poor or noisy so that data do not allow to estimate reliably terms $\gamma$ and $\delta$, these can be neglected, and then Eqs. (4) become

$$V_{\rm c}^{\rm iso} = \sigma_{\rm iso}(R)\sqrt{\alpha+1}\,,$$
$$V_{\rm c}^{\rm circ} = \sigma_{\rm circ}(R)\sqrt{2\frac{\alpha+1}{\alpha}}\,, \quad (6)$$
$$V_{\rm c}^{\rm rad} = \sigma_{\rm rad}(R)\sqrt{\alpha^2-1}\,.$$

At a radius where all three profiles $V_{\rm c}^{\rm iso}$, $V_{\rm c}^{\rm circ}$, and $V_{\rm c}^{\rm rad}$ intersect (or are close to) each other – a sweet point $R_{\rm sweet}$ – the sensitivity of the method to the anisotropy is minimal. The sweet point is expected to be not far from a radius $R_2$ where the surface brightness slope $\alpha = -{\rm d}\ln I/{\rm d}\ln R = 2$. For example, in case of $I(R) \propto R^{-2}$, $\beta = {\rm const}$ and nearly flat $\sigma_{\rm p}$-profile (so using the Eqs. 6 is justified) the resulting circular speed $V_{\rm c}$ is independent of the anisotropy parameter (Gerhard 1993). Let us also note that $R_2$ is close (within a factor of $\sim 2$) to the half-light radius $R_{\rm eff}$ of tracers so $R_{\rm sweet} \sim R_2 \sim R_{\rm eff}$.

Let us emphasize that relations (4) and (6) appear to be approximately valid even if the gravitational potential $\Phi(r)$ is not purely isothermal and/or $\beta$ slowly varies with radius (Lyskova et al. 2012). The derivation of all Eqs. (4)–(6) can be found in Churazov et al. (2010) and Lyskova et al. (2012).

## 3 An algorithm for estimating $V_{\rm c}$

1. Calculate the logarithmic derivatives $\alpha$, $\gamma$, and $\delta$ from the observed surface brightness $I(R)$ and line-of-sight velocity dispersion $\sigma_{\rm p}(R)$ profiles.
2. Calculate the circular speed $V_{\rm c}(R)$ for isotropic, radial and circular orbits of tracer particles using Eqs. (4) in case of reliable data (full analysis) or Eqs. (6) in case of missing or noisy observational data (simplified analysis).
3. Estimate $V_{\rm c}$ as $V_{\rm c}^{\rm iso}(R_{\rm sweet})$ at the sweet spot $R_{\rm sweet}$ – the radius at which all three curves $V_{\rm c}^{\rm iso}(R), V_{\rm c}^{\rm circ}(R)$, and $V_{\rm c}^{\rm rad}(R)$ are maximally close to each other. At $R_{\rm sweet}$ the sensitivity of the method to the anisotropy parameter $\beta$ is believed to be minimal so the estimation of the circular speed at this particular point is not affected much by the unknown distribution of tracers' orbits.

## 4 Testing the method on simulated elliptical galaxies

To test the described procedure we have applied it to (i) a sample of simulated elliptical galaxies and (ii) to a sample of simulated galaxy clusters. For the circular speed determination of ellipticals we have used stars as tracers (also planetary nebulae and globular clusters can be used). To estimate masses of galaxy clusters we have used the spatial distribution and velocity dispersion of individual subhalos (= galaxies).

### 4.1 Description of the sample of simulated galaxies

To test the method we have applied it to a sample of 65 simulated galaxies described in detail in Oser et al. 2010. Three independent projections of each galaxy have been considered to increase effectively the number of objects in the sample. We characterize the accuracy of the method via deviation from the true circular speed $\Delta_{\rm opt} = \left(V_{\rm c}^{\rm iso} - V_{\rm c}^{\rm true}\right)/V_{\rm c}^{\rm true}$, where $V_{\rm c}^{\rm iso}$ and $V_{\rm c}^{\rm true}$ should be taken at the sweet radius $R_{\rm sweet}$. The subscript "opt" (= optical) is introduced here to distinguish this method from mass calculations based on X-ray data.

Let us illustrate all steps of the described algorithm on one simulated galaxy with code name "M0125" (Fig. 1) from Oser et al. (2010). This object is quite massive (stellar mass $M_* \simeq 3.1\times10^{11}\,h^{-1}\,{\rm M}_\odot$, $h = 0.72$) with an effective radius $R_{\rm eff} = 14.4$ kpc. After excluding satellites from the galaxy image we have computed the surface brightness and the line-of-sight velocity dispersion profiles in a set of concentric annuli around the halo center (Fig. 1, red dots in panels A and B) and calculated logarithmic derivatives $\alpha$, $\gamma$ and $\delta$ (Fig. 1, panel C). Using Eqs. 4 we have computed $V_{\rm c}$-profiles assuming three types of orbits: isotropic ($V_{\rm c}^{\rm iso}$), radial ($V_{\rm c}^{\rm rad}$) and circular ($V_{\rm c}^{\rm circ}$). Then we have found the sweet point $R_{\rm sweet}$ as the radius at which the quantity $(V_{\rm c}^{\rm iso} - \overline{V})^2 + (V_{\rm c}^{\rm rad} - \overline{V})^2 + (V_{\rm c}^{\rm circ} - \overline{V})^2$, where $\overline{V} = (V_{\rm c}^{\rm iso} + V_{\rm c}^{\rm rad} + V_{\rm c}^{\rm circ})/3$, is minimal. We use $V_{\rm c}^{\rm iso}(R_{\rm sweet})$ as the estimate of the circular velocity. For this particular example the estimated $V_{\rm c}$ deviates from the true one by only 1 %.

Since the method under consideration was primarily designed for massive elliptical galaxies we have estimated the bias and the scatter for the subsample of massive ellipticals ($\sigma_{\rm p}(R_{\rm eff}) > 150$ km s$^{-1}$), excluding merging and oblate objects observed along the rotation axis (subsample "MG"). As can be seen from Fig. 2 the $V_{\rm c}$-estimate at the sweet point via Eqs. (4) is almost unbiased when averaged over the subsample ($\overline{\Delta_{\rm opt}} < 1$ %) and rms-scatter is reasonable $\simeq$ 5–8 % for nearby as well as distant galaxies. Therefore the discussed procedure suits well for quick and robust mass estimates of large samples of galaxies (e.g., galaxy surveys) both at low and high redshifts.

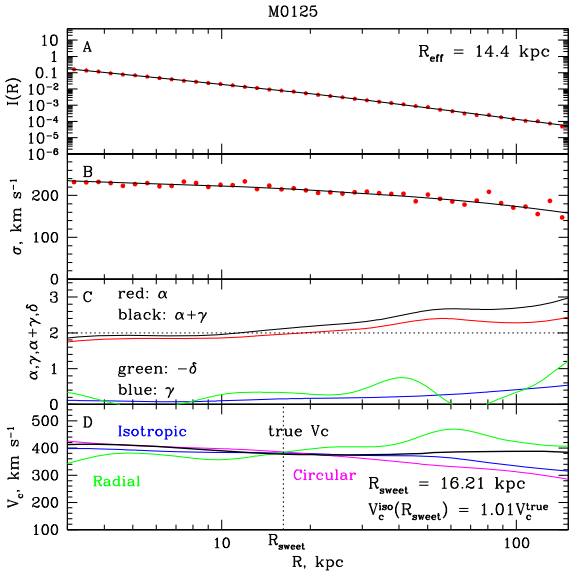


**Fig. 1** Circular speed estimation in the simulated elliptical galaxy. The surface brightness and the line-of-sight velocity dispersion profiles are shown in *panels A and B* correspondingly (data are shown as red points, smoothed curves used for computing logarithmic derivatives $\alpha, \gamma, \delta$ as black solid lines). The coefficients $\alpha, \gamma, -\delta$ and $\alpha+\gamma$ are shown in *panel C* in red solid, blue dotted, green dash-dotted and black dashed lines, respectively. Circular speed profiles for isotropic stellar orbits (blue solid line), pure radial (green dash-dotted) and pure circular (magenta dashed) orbits as well as the true circular speed (black thick curve) are presented in *panel D* for the full version of the analysis (Eqs. 4).

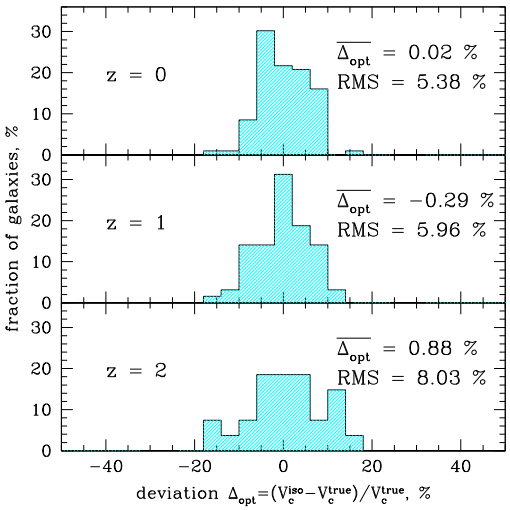


**Fig. 2** Distribution of galaxies from the subsample "MG" (massive objects with $\sigma(R_{\rm eff}) > 150$ km s$^{-1}$, merging and oblate galaxies observed along the rotation axis are excluded) at different redshifts: $z = 0$ (*top*), $z = 1$ (*middle*), $z = 2$ (*bottom*) according to their circular speed deviations.

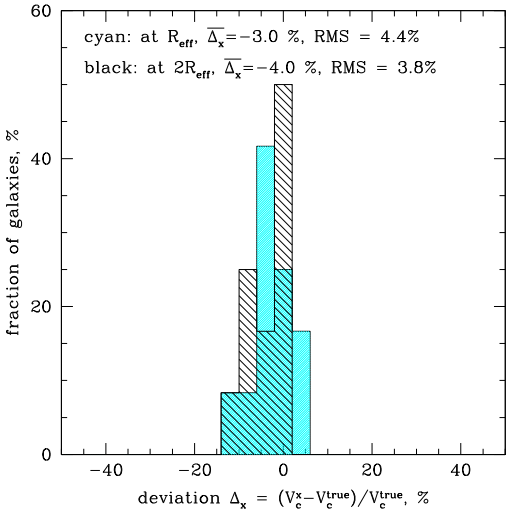


**Fig. 3** Distribution of the most massive galaxies with $M > 6.5\times10^{12}$ M$_\odot$ according to their deviations of the estimated circular speed $V_c^x$ from the true value at $R_{\rm eff}$ (cyan histogram) and at $2R_{\rm eff}$ (black histogram). $V_c^x$ is derived using the hydrostatic equilibrium equation.

### 4.2 Circular speed from X-ray data

Using the same set of simulated galaxies we have also tested how accurate is the circular speed estimate $V_c^x$ from the hydrostatic equilibrium equation. To estimate the mass bias that comes from the assumption of the gas hydrostatic equilibrium we have analyzed a subsample of most massive ellipticals in the sample ($M > 6.5\times10^{12}\,\mathrm{M}_\odot$). The resulting subsample consists of 12 galaxies. To characterize deviations from the hydrostatic equilibrium we have calculated $\Delta_X = (V_c^x - V_c^{\rm true})/V_c^{\rm true}$ at two radii: $R_{\rm eff}$ and $2R_{\rm eff}$ (cyan and black histograms in Fig. 3, respectively). The average deviation is biased low by 3–4 % and the scatter is $\simeq$5 %. The observed mass bias can be traced to the residual gas motions.

## 5 Testing the method on simulated galaxy clusters

Let us now apply the method to a set of simulated clusters of galaxies. As tracer particles we can use individual galaxies. We have performed the same analysis for a sample of simulated halos from Dolag et al. (2009). Extracted light profile (number of galaxies per unit area) and line-of-sight velocity dispersion profile have much more scatter than those for the elliptical galaxies due to smaller number of tracers. So it is reasonable to use the simplified version of the analysis (Eqs. 6).

Figure 4 illustrates an example of applying the method to a simulated galaxy cluster. The projected number density $I(R)$ and the line-of-sight velocity dispersion profiles are shown in Fig. 4, panels A and B. Using Eqs. (6) we have computed $V_c^{\rm iso}$, $V_c^{\rm rad}$, and $V_c^{\rm circ}$ and found a point $R_{\rm sweet}$ of their intersection at which we estimate the circular speed and calculated the deviation $\Delta_{\rm opt}$.

Figure 5 shows the histograms of the deviation $\Delta_{\rm opt}$ for two cases: when number of galaxies (subhalos) is large, e.g.

 

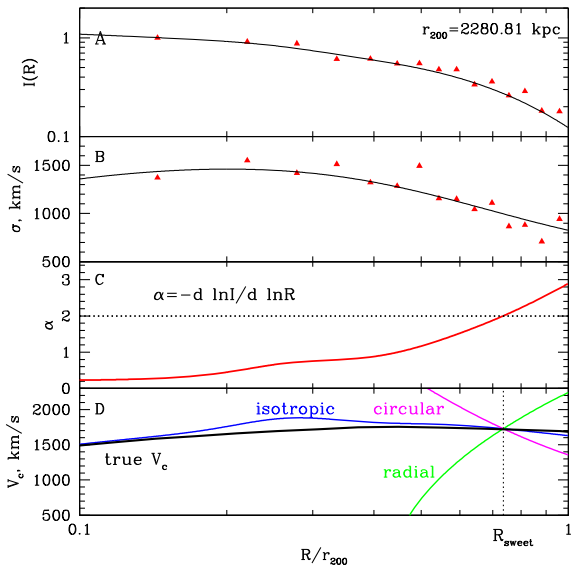


**Fig. 4** Circular speed estimation in the simulated galaxy cluster. The projected number density of galaxies and the line-of-sight velocity dispersion profiles are shown in *panels A and B*, respectively (data are shown as red triangles, interpolated curves as black solid lines). The slope of the surface brightness $\alpha$ is shown in *panel C* as a red solid line. Circular speed profiles for isotropic orbits of galaxies (blue solid line), pure radial (green dash-dotted) and pure circular (magenta dashed) orbits as well as the true circular speed (black thick curve) are shown in *panel D* for the simplified version of the analysis (Eqs. 6).

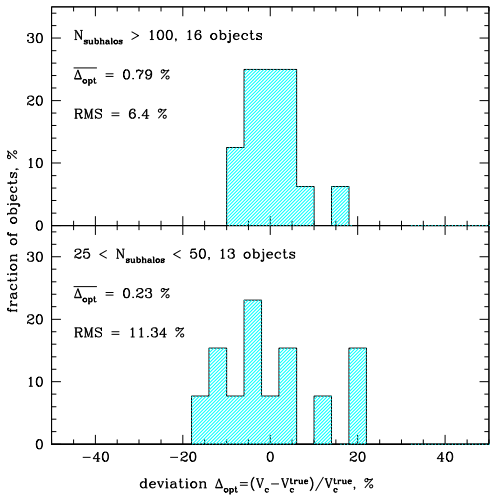


**Fig. 5** The fraction of galaxy clusters as a function of the deviation $\Delta_{\rm opt}$ for two cases: rich (*top*) and small clusters (*bottom*).

$N_{\rm subhalos} > 100$ (Fig. 5, top panel), and when the number of galaxies does not exceed 50 (Fig. 5, bottom panel).

When averaged over a sample the deviation is close to zero which allows one to use the method for mass determination of even small clusters with $\sim$30–50 data points available and for cross-calibration of other mass determination methods (X-ray analysis, weak lensing, etc.).

## 6 Conclusion

We have discussed the technique for determination of the mass enclosed within some particular radius – the sweet point $R_{\rm sweet}$ – where the mass uncertainty due to the unknown anisotropy of tracers' orbits is minimal. The sweet spot is expected to be located not far from the radius $R_2$ where the surface brightness declines as $R^{-2}$ which is in turn close to the half-light radius $R_{\rm eff}$. The method is based on the most basic observables such as the surface brightness and the line-of-sight velocity dispersion and does not require any assumptions about tracers' orbits or mass profile to be made. To test the performance of the method we have applied it to a set of simulated individual galaxies and galaxy clusters and calculated the bias and the scatter of the recovered circular speed.

For massive elliptical galaxies ($\sigma_{\rm p}(R_{\rm eff}) > 150\,{\rm km\,s^{-1}}$) without signs of significant rotation the discussed procedure provides an unbiased estimate ($\overline{\Delta}_{\rm opt} < 1\,\%$) of the circular speed when averaged over a sample with rms-scatter = 5–6 %. For simulated ellipticals at higher redshifts (namely, at $z = 1$ and $z = 2$) the average deviation $\overline{\Delta}_{\rm opt}$ of the recovered circular speed from the true one is still close to zero while the rms-scatter becomes slightly larger, up to 8 %.

When applying the method to galaxy clusters it is reasonable to use the simplified version of the analysis (Eq. 6) as the number of tracers (and, as a consequence, the number of data points) is much smaller than in the case of galaxies. However, the recovered circular speed estimate remains almost unbiased for poor as well as rich galaxy clusters with a reasonable scatter, e.g. rms = 11.3 % for objects containing 25–30 tracer particles and rms reduces to 6.4 % when more than 100 tracers available.

Given it's simplicity, small bias and modest scatter the method can be applied for quick mass estimations for large samples of elliptical galaxies and galaxy clusters especially when the comprehensive study of each individual object is not justified.

## References

Binney, J., & Tremaine, S. 2008, Galactic Dynamics, 2nd ed. (Princeton University Press)
Churazov, E., Tremaine, S., Forman, W., et al. 2010, MNRAS, 404, 1165
Dolag, K., Borgani, S., Murante, G., & Springel V. 2009, MNRAS, 399, 497
Gebhardt, K., & Thomas, J. 2009, ApJ, 700, 1690
Gerhard, O. E. 1993, MNRAS, 265, 213
Lyskova, N., Churazov, E., Zhuravleva, I., et al. 2012, MNRAS, 423, 1813
Oser, L., Ostriker, J. P., Naab, T., Johansson, P. H., & Burkert, A. 2010, ApJ, 725, 2312
Richstone, D. O., & Tremaine, S. 1984, ApJ, 286, 27
Schwarzschild, M. 1979, ApJ, 232, 236
Wolf, J., Martinez, G. D., Bullock, J. S., et al. 2010, MNRAS, 406, 1220